Accepted Manuscript

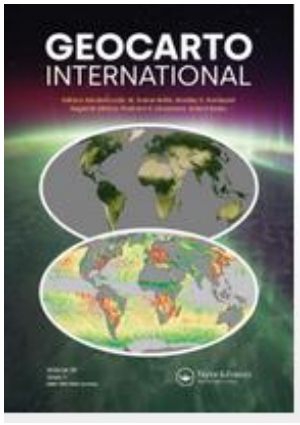

Estimation of Actual Evapotranspiration using TDTM model and MODIS derived variables

Marcos Ruiz-Álvareza, Francisco Gomariz-Castillo, Francisco Alonso-Sarría and Ana López-Ballesteros

DOI: https://doi.org/10.1080/10106049.2021.2017011
Reference: 215980445

To appear in: *Geocarto International*

Received date: 2 August 2021
Accepted date: 5 December 2021
Published online: 10 January 2022
Final publication: 10 January 2022

Marcos Ruiz-Álvarez, Francisco Gomariz-Castillo, Francisco Alonso-Sarría & Ana López-Ballesteros (2022) Estimation of actual evapotranspiration using TDTM model and MODIS derived variables, Geocarto International, 37:25, 9242-9260, DOI: 10.1080/10106049.2021.2017011

Correspondence to Francisco Gomariz-Castillo

Estimation of Actual Evapotranspiration using TDTM model and MODIS derived variables

Marcos Ruiz-Álvarez[a]*, Francisco Gomariz-Castillo [ab]*, Francisco Alonso-Sarría[ab] and Ana López-Ballesteros[c]

[a]*Instituto Universitario de Agua y Medio Ambiente, University of Murcia, Murcia, Spain;* [b]*Department of Geography, University of Murcia, Murcia, Spain;* [c]*Basque Centre for Climate Change, Leioa, Basque, Spain*

* Corresponding author. Email: fjgomariz@um.es. Campus de Espinardo s/n 30100. Murcia, Spain. Telephone number: +34 868888695.

Estimation of Actual Evapotranspiration using TDTM model and MODIS derived variables

Abstract: The objective of this paper is to contribute to improve ETa estimation in semiarid environments by proposing two variations to the TDMT model. These variations are based on the use of MODIS products from TERRA or AQUA satellites and on the use of NDVI instead of EVI, to estimate the fraction of vegetation cover. The proposed changes were validated with the original methodology for the 2012-2014 period with data obtained from two flux towers (ES-LJu and ES-Amo). The best results were obtained when using the alternative methodology (RMSE of 0.64-0.67 mm in ES-Lju and of 0.97-1.02 mm in ES-Amo). Additionally, a correction of the temporal systematic errors of the model based on Random Forest is proposed. With this correction, RMSE of 0.31-0.35 mm in ES-Lju and 0.30-0.34 mm in ES-Amo were obtained. The spatial distribution obtained with this corrected model is the most consistent with the characteristics of the study area.

Keywords: actual evapotranspiration; MODIS; TDTM; flux towers; Random Forest

1. Introduction

Actual evapotranspiration (ETa) is the amount of water evaporated and transpired under existing conditions. It is one of the most important processes in the water cycle and is differently influenced by various meteorological variables, such as precipitation, temperature or humidity of the soil and air, in different climatic regions (Yaseen *et al.* 2020), in addition to other factors such as vegetation cover and soil conditions. Accurate estimation of ETa is of particular interest in semi-arid regions, where water scarcity represents the main obstacle to agricultural production, economic well-being or sustainable development (Jamshidi *et al.* 2019a, Jamshidi *et al.* 2019b). An accurate and spatially distributed estimation of ETa is essential to improve water resources management (Yang *et al.* 2012), drought monitoring and assessment (Senay *et al.* 2013,

Lorenz *et al.* 2017), irrigation scheduling (Pereira *et al.* 2015), soil and water salinity problems associated with irrigated agriculture management in semi-arid areas (Minhas *et al.* 2020), calibration and validation of hydrological models (Herman *et al.* 2018) or the quantification of aquifer recharge (Beigi and Tsai 2014).

The estimation of ETa is rather complicated due to the large number of factors involved (Glenn *et al.* 2007). ETa can be measured at local scale using micrometeorological methods (Bowen ratio and eddy covariance system) or soil water balance (lysimeters). However, this approach is limited to areas smaller than 1 km^2 (Allen *et al.* 2011). The availability of the variables needed to estimate ETa as remote sensing products has boosted the development of new methods more feasible and cost-effective both at regional (Xiong *et al.* 2015) and global scales (Mu *et al.* 2011).

Kalma *et al.* (2008), Li *et al.* (2009) and Zhang *et al.* (2016) review such methods. Most of them are based on the surface energy balance (SEB methods), in which ETa is estimated as a residual of the surface energy balance. The SEB methods are divided into one-source and two-source methods. The latter allows to discriminate between soil evaporation and vegetation transpiration. Examples of one-source SEB methods are: Surface Energy Balance Algorithm for Land (SEBAL) (Teixeira *et al.* 2009a, Teixeira *et al.* 2009b, Rahimpour and Rahimzadegan 2021), Mapping Evapotranspiration at High Resolution with Internalized Calibration (METRIC) (Allen *et al.* 2007a, Allen *et al.* 2007b, Jamshidi *et al.* 2019a), Simplified Surface Energy Balance Index (S-SEBI) (Roerink *et al.* 2000), Surface Energy Balance System (SEBS) (Su 2002, Jamshidi *et al.* 2019b) and operational Simplified Surface Energy Balance (SSEBop) (Senay *et al.* 2013, Niyogi *et al.* 2020, Rahimpour and Rahimzadegan 2021). Two-Source Methods (TSM) include: TSM scheme (TSMN) (Norman *et al.* 1995), Atmosphere-Land Exchange Inverse (ALEXI) (Anderson *et al.* 2007), flux disaggregation approach of ALEXI

(disALEXI) (Norman *et al.* 2003) and Three-Temperature (3T) (Xiong and Qiu 2014, Xiong *et al.* 2015).

Empirical methods based on the Penman-Monteith equation, such as MOD16 (Mu *et al.* 2011, Gavahi *et al.* 2020, Wang *et al.* 2021) or Priestley-Taylor (Niyogi *et al.* 2020, Pourmansouri and Rahimzadegan 2020) have also been developed; MOD16 being one of the most widely used.

Another approach is the use of graphical methods based on the interpretation of the scatter plot of surface temperature and vegetation indices (hereinafter Ts-VI space) (Zhu *et al.* 2017). Generally, the Ts-VI space is triangular, so these graphical methods are also known as triangle methods.

The Time-Domain Triangle Method (TDTM) is based on the interpretation of the scatter plot between the daily thermal amplitude and the Enhanced Vegetation Index (EVI) (Minacapilli *et al.* 2016). All the input data required, with the exception of air temperature, are derived from satellite imagery (MODIS sensor), which makes it suitable for estimating ETa in arid and semi-arid areas. It is based on the triangle method, first developed by Price (1990) and later modified by Jiang and Islam (2001) to allow its use with remotely sensed imagery. The feature space characteristic of the triangle method is defined by the daily thermal amplitude (difference between the surface temperature estimated by the MODIS sensor in the daytime and nighttime images of the TERRA satellite) and the EVI. The TDTM model was applied in Sicily (Italy) and its results were validated using ETa values estimated from the variables measured in 2 flux towers (Minacapilli *et al.* 2016).

The objective of this paper is to contribute to improve ETa estimation in semi-arid environments proposing three main innovations. First and foremost, the proposal of two variations of the TDTM model based on an alternative methodology for the

calculation of the vegetation cover fraction (F_C) using NDVI instead of EVI and on the use of MODIS products from the AQUA and TERRA satellites. The second innovation is the use of Random Forest for the correction of systematic errors. The third is the proposal of the study itself as a framework to estimate ETa in a spatially distributed way from freely available information. We compare the accuracy of the modifications and of the original TDTM method by using observed ETa values at a daily scale in the period 2012-2014 and in 2 flux towers, which are part of the FLUXNET network, located in the province of Almeria, in the vicinity of the study area.

2. Methodology

2.1. Study area

Our study was carried-out in the area managed by the River Segura Water Authority (DHS) (Figure 1). It is a semiarid area with scarce and irregular precipitation, high temperature, and high potential evapotranspiration. The mean annual precipitation is 375 mm/year (CHS 2015), being therefore one of the driest regions in continental Europe. However, its spatial distribution is closely related to relief, the highest precipitation values are registered in the extreme northwestern of the DHS with an annual average slightly higher than 1000 mm. Precipitation descends drastically in a northwest-southeast direction reaching 200-250 mm/year in the southwestern coast of the study area. On the other hand, the annual potential evapotranspiration in DHS ranges between 1100 and 1400 mm / year, registering in most of the DHS (83%) values between 1200 and 1300 mm / year with an average of 1258 mm (Gomariz-Castillo 2016).). Despite the scarcity of water, agriculture is an important economic sector. Population density and intensive irrigated agriculture represent a significant water demand.

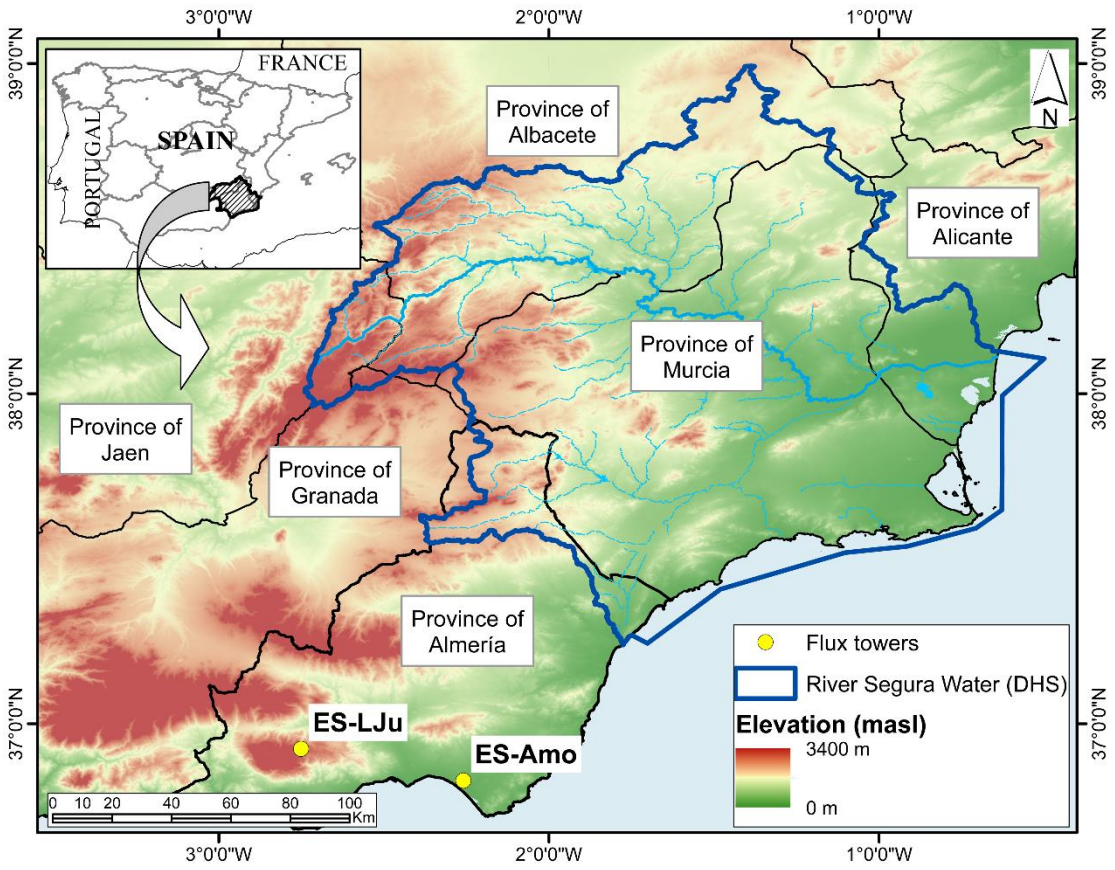

Figure 1. Study area and location of the flow towers used to validate the TDTM model and the proposed variations.

Altitude strongly influences the spatial distribution of temperature. The annual average temperature increases gradually from the Northwest mountain ranges (10 ºC) to the coast (18 ºC). The proximity to the sea softens summer and winter temperatures in the coast, while continental climatic features appear towards the interior area because of the distance to the sea and the presence of successive mountain alignments (Conesa-García and Alonso-Sarría 2006). Cloudiness increases in the equinoctial seasons, since anticyclonic situations are common in winter and summer.

The soils of the study area are characterized by a large diversity because of the combination of climatic, lithological, topographic, anthropic and biotic factors. Leptosols, Regosols, Fluvisols and Cambisols are the most common soil type in DHS.

Scrubs and grasslands occupy, according to data from the Corine Land Cover 2018 project, the 27 % of the DHS and are their most common vegetation type. This data is important, since this is the area that most closely resembles the vegetation present in the 2 flow towers used. After scrubs and grasslands, forests and permanent crops with 18.5% each one, are the most common land cover in DHS.

2.2. Remote sensing data

The following MODIS derived products (version 6) are needed to apply the TDTM model: MOD11A1 (Wan *et al.* 2015a), MYD11A1 (Wan *et al.* 2015c), MOD11A2 (Wan *et al.* 2015b), MYD11A2 (Wan *et al.* 2015d), MOD13Q1 (Didan 2015), MYD13Q1 (Myneni *et al.* 2015) and MCD43A3 (Schaaf and Wang 2015). Table 1 lists their main characteristics. The layers of these products were obtained using the MODIStsp R (Myneni *et al.* 2015), which allows to automate their download and processing. The data acquired by the MODIS sensor are grouped into 1200 x 1200 km tiles. The study area of this work corresponds to tile v5h17.

Table 1. Main characteristics of the products derived from the MODIS sensor: $T_{sup,day}$ is daily temperature; ε_0 is emissivity; α is albedo; NDVI is the normalized difference vegetation index; and EVI is the enhanced vegetation index.

Sensor	**Platform**	**Layer**	**Name**	**Spatial resolution (km)**	**Temporal resolution (days)**
MODIS	Terra	$T_{sup,day}$	MOD11A1	1	1
MODIS	Aqua	$T_{sup,day}$	MYD11A1	1	1
MODIS	Terra	ε_0	MOD11A2	1	1
MODIS	Aqua	ε_0	MYD11A2	1	1
MODIS	Terra and Aqua	α	MCD43A3	0.5	1 (Average 16 days)
MODIS	Terra	NDVI,EVI	MOD13Q1	0.25	16
MODIS	Aqua	NDVI,EVI	MYD13Q1	0.25	16

2.3. Flux towers data

Data from two flux towers located in scrub areas in the province of Almeria, bordering the study area (Figure 1), were used to validate the estimated values of ETa : Amoladeras (ES-Amo) and Llano de los Juanes (ES-LJu). Both are part of the FLUXNET (Pastorello *et al.* 2020). The characteristics of ES-LJu are described in Serrano-Ortiz *et al.* (2007) and Serrano-Ortiz *et al.* (2009) whereas those of ES-Amo are described in López-Ballesteros *et al.* (2017). Both are surrounded by scrub areas, the soil type in ES-LJu is a Lithic Haploxeroll (aridic soil moisture) and Leptosol in ES-Amo. So, both flux towers can be representative of the environment in most of the River Segura basin. Observed ETa data from both flux towers for the period 2012 - 2014 were used. The series is complete for ES-LJu, but only 57% of the days are available for ES-Amo. In addition to the ETa data, the managers of both flux towers also provided air temperature data, which will be used as input for the calculation of ETa using the 3T and TDTM models in both flux towers.

In both flux towers, latent heat flux (LHF) measurements are made every 30 minutes, so each instantaneous observation averages the 30-minute interval prior to the observation. These values were aggregated for the period from dawn to dusk to obtain ETa values on a daily scale assuming, as in Cleugh *et al.* (2007) and García *et al.* (2014), that ETa during the night period is negligible.

Figure 2 shows the daily values of ETa in the ES-LJu and ES-Amo flux towers in the 2012-2014 period. ES-Amo. Table 2 shows the monthly average daily ETa for ES-LJu and ES-Amo. The highest values are reached between April and July (especially in June). In the rest of the months the average daily ETa is less than 0.5 mm.

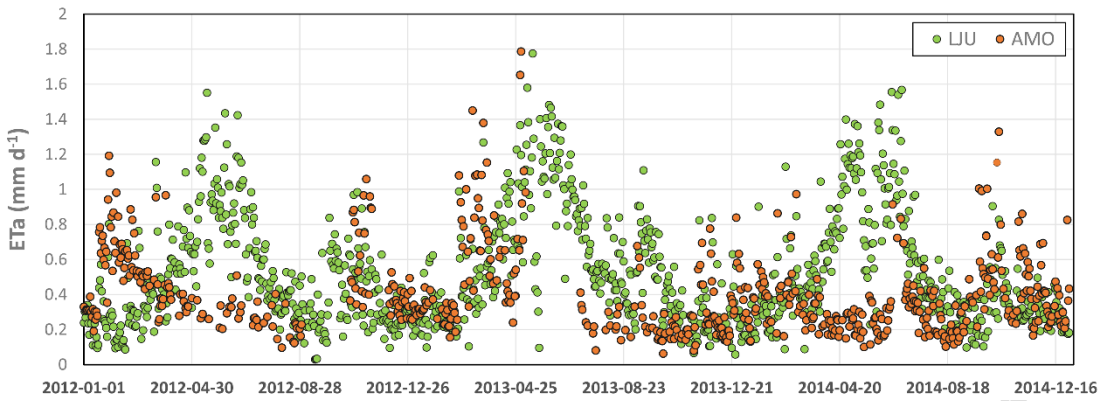

Figure 2. Daily ETa values measured in the ES-LJu y ES-Amo flux towers (2012-2014).

Table 2. Monthly average of daily ETa (mm d^{-1}) in ES-LJu and ES-Amo flux tower (2012-2014). The percentage of missing data for each month is shown in parentheses for ES-Amo.

	Jan.	**Feb.**	**Mar.**	**Apr.**	**May.**	**Jun.**	**Jul.**	**Aug.**	**Sep.**	**Oct.**	**Nov.**	**Dec.**
ES-LJu	0.29	0.33	0.48	0.75	0.95	1.05	0.6	0.4	0.38	0.43	0.34	0.27
ES-Amo	0.42	0.52	0.56	0.4	0.38	0.35	0.31	0.22	0.4	0.41	0.47	0.34
%	(27)	(26)	(32)	(41)	(64)	(70)	(53)	(49)	(63)	(49)	(30)	(14)

2.4. TDTM model

This section describes the methodology used to estimate ETa with the TDTM model using surface temperature data obtained at both the TERRA and AQUA satellite passage times. A flowchart of this methodology is shown in Figure 3.

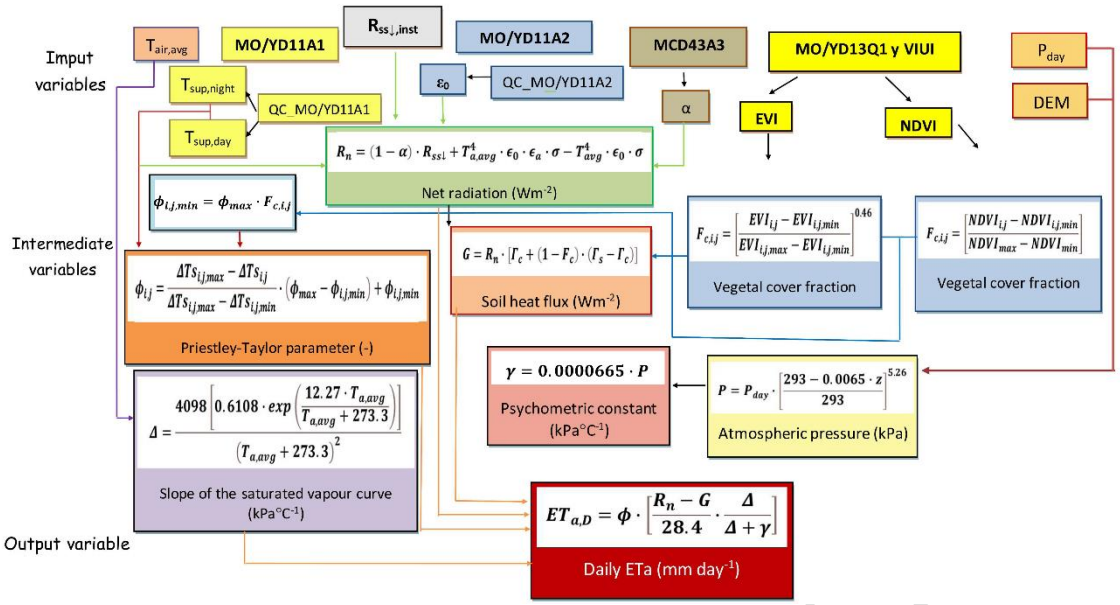

Figure 3. TDTM model flow chart.

In the TDTM model, the calculation of the real daily evapotranspiration (mm d^{-1}) is carried out using the Priestley-Taylor equation (Priestley and Taylor 1972):

$$ET_{a,D} = \phi \cdot \left[\frac{R_n - G}{28.4} \cdot \frac{\Delta}{\Delta+\gamma}\right] \quad (1)$$

Where ϕ is the Priestley-Taylor parameter (Equation (2)); R_n is the daily mean net radiation (Equation (6)); G is the daily mean heat flux (Equation (10)); Δ is the slope of the saturated vapour pressure versus air temperature curve (kPa $^oC^{-1}$) (Equation (11)) and γ is the psychrometric constant (kPa $^oC^{-1}$) (Equation (12)). The factor 28.4 is used to convert the available energy (R_n - G) from (W/m^2) to mm d^{-1}. In Equation (1), $\frac{\Delta}{\Delta+\gamma}$ represents the evaporative fraction (ratio of actual evapotranspiration to available energy).

2.4.1. Priestley-Taylor parameter calculation

Equations (2) to (4) show the process to estimate the ϕ parameter for each pixel according to Minacapilli *et al.* (2016):

$$\phi_{i,j} = \frac{\Delta Ts_{i,j,max} - \Delta Ts_{i,j}}{\Delta Ts_{i,j,max} - \Delta Ts_{i,j,min}} \cdot \left(\phi_{max} - \phi_{i,j,min}\right) + \phi_{i,j,min} \quad (2)$$

$$\phi_{i,j,min} = \phi_{max} \cdot F_{c,i,j} \quad (3)$$

The suffixes *i,j* refer to the generic pixel; $\Delta Ts_{i,j,max}$ and $\Delta Ts_{i,j,min}$ are the daily maximum and minimum thermal amplitude in the analysed period. In this case the daily thermal amplitude is defined as the difference between the surface temperature provided by the MODIS sensor in the daytime and nighttime passage times of the TERRA and AQUA satellites; and $\Delta Ts_{i,j}$ is the daily thermal amplitude. Minacapilli *et al.* (2016) justify this variation on the grounds that the daily surface thermal amplitude is a good estimator of the resistance of the surface to external temperature variations. Therefore, a wet soil will have a higher resistance to temperature variation than a dry soil, and therefore a lower thermal amplitude.

The parameter ϕ_{max} in the original Priestley-Taylor equation is assumed to be equal to 1.26 (Priestley and Taylor 1972). However, Minacapilli *et al.* (2016) propose to use a value of 1.35 in semi-arid areas. This paper will compare the results obtained with both values.

In this study, the fraction of vegetation cover for each pixel (F_c). is obtained using 2 methods: 1) The reference method proposed by Minacapilli *et al.* (2016) that is based on the EVI index (Equation (4)) and 2) the method proposed by Carlson *et al.* (1995), based on the NDVI index (Equation (5)). The second methodology has been widely used to estimate ETa in semiarid environments (Tang *et al.* 2010, Tian *et al.* 2013, Zhou *et al.* 2014) and has been applied in this work, due to poor results obtained with the reference methodology in a preliminary study. Onwards the first and second methodologies will be called FC-EVI and FC-NDVI respectively.

$$F_{c,i,j} = \left[\frac{EVI_{i,j} - EVI_{i,j,min}}{EVI_{i,j,max} - EVI_{i,j,min}}\right]^{0.46} \quad (4)$$

$$F_{c,i,j} = \left[\frac{NDVI_{i,j} - NDVI_{i,j,min}}{NDVI_{max} - NDVI_{min}}\right] \quad (5)$$

$EVI_{i,j}$ is the EVI value to each pixel; $EVI_{i,j,max}$, $EVI_{i,j,min}$ are the maximum and minimum EVI values estimated for each pixel over the entire study period, $NDVI_{max}$ is equal to 0.86 (Prihodko and Goward 1997), $NDVI_{min}$ is equal to 0.2 (Tang *et al.* 2010) and $NDVI_{i,j}$ is the NDVI corresponding to each pixel.

2.4.2. Surface net radiation and heat flux from the ground

To calculate the net radiation (R_n) we used the methodology proposed by Minacapilli *et al.* (2016) with some variations:

$$R_n = R_{ss\downarrow} - R_{ss\uparrow} + R_{sl\downarrow} - R_{sl\uparrow} = (1-\alpha)\cdot R_{ss\downarrow} + T_{a,avg}^4 \cdot \epsilon_0 \cdot \epsilon_a \cdot \sigma - T_{avg}^4 \cdot \epsilon_0 \cdot \sigma \quad (6)$$

$R_{ss\downarrow}$, $R_{ss\uparrow}$, $R_{sl\downarrow}$ and $R_{sl\uparrow}$ represent in W/m^2 the incoming shortwave, outgoing shortwave, incoming longwave and outgoing longwave radiation, respectively. $T_{a,avg}$ is the daily mean air temperature and T_{avg} is the daily mean surface temperature (obtained from the average of the surface temperature estimated in the nighttime and daytime passes of both satellites). α, ϵ_a and ϵ_0 are the albedo, air emisivity and soil emisivity, respectively.

Daily $T_{a,avg}$ layers were obtained from Ruiz-Álvarez *et al.* (2020). The method used to obtain $T_{a,avg}$ values also differs from the one used in the original TDTM model. Minacapilli *et al.* (2016) obtained $T_{a,avg}$ is from the incoming longwave solar radiation and atmospheric emissivity whereas Ruiz-Álvarez *et al.* (2020) obtained it using machine learning based predictive models.

The Daily Downward Surface Shortwave Flux (DIDSSF LSA-09) SEVIRI product were not used as $R_{ss\downarrow}$ layers as in Minacapilli *et al.* (2016). They were obtained following the methodology described in Allen *et al.* (2006):

$$R_{ss\downarrow} = \tau \cdot R_a \tag{7}$$

$$R_a = \frac{G_{SC} \cdot d_T \cdot [\omega sin\varphi sin\delta + cos\varphi sin\omega]}{\pi} \tag{8}$$

Where R_a is the extraterrestrial radiation, τ is the atmospheric transmissivity, G_{SC} is the solar constant (1367 W/m^2), d_T is the inverse of the relative Earth-Sun distance, ω is the angle of radiation at sunset (radians), φ is the latitude in radians and δ is the solar declination. Both δ and d_T depend on the Julian day (Allen et al., 2006). Finally, ω is obtained according to Allen *et al.* (2006) as:

$$\omega_s = arccos[-tan\varphi tan\delta] \tag{9}$$

The heat flux from the ground is obtained as:

$$G = R_n \cdot [\Gamma_c + (1 - F_c) \cdot (\Gamma_s - \Gamma_c)] \tag{10}$$

The parameter Γ_c is equal to 0.05 (Monteith and Unsworth 2013) and Γ_S is equal to 0.315 (Kustas and Daughtry 1990).

2.4.3. Calculation of Δ and γ

Equations (11) and (12) show the calculation of the slope of the saturated vapour pressure versus air temperature curve (Δ) and of the psychrometric constant (γ) (Allen *et al.* 2006):

$$\Delta = \frac{4098\left[0.6108 \cdot exp\left(\frac{12.27 \cdot T_{a,avg}}{T_{a,avg}+273.3}\right)\right]}{\left(T_{a,avg}+273.3\right)^2} \tag{11}$$

$$\gamma = 0.0000665 \cdot P \quad (12)$$

$T_{a,avg}$ is the daily mean air temperature in ºC and P is the atmospheric pressure (Equation (13)) whose spatially distributed values are obtained from the elevation above sea level (z) in metres, according to Allen *et al.* (2006).

$$P = 101.3 \cdot \left[\frac{293 - 0.0065 \cdot z}{293}\right]^{5.26} \quad (13)$$

In summary, tTwo variations to the methodology proposed by Minacapilli *et al.* (2016) to estimate Eta are proposed: Changing both the surface temperature used (estimated using TERRA or AQUA) and the method to calculate the fraction of vegetation cover used (FC-EVI or FC-NDVI). Below are shown the main characteristics and the name (between parenthesis) of each of the proposed variations and of the reference methodology:

- Reference methodology: use of FC-EVI and TERRA (TDTM-EVI-O model).
- 1st Variation: use of FC-EVI and AQUA (TDTM-EVI-Y model).
- 2nd Variation: use of FC-NDVI and TERRA (TDTM-NDVI-O model).
- 3rd Variation: use of FC-NDVI and AQUA (TDTM-NDVI-Y model).

2.4.4. Correction of model errors

In order to correct systematic errors related to the daily thermal amplitude, especially in Summer, we used a Random Forest (RF) model (Breiman 2001) to reproduce this effect and correct the ETa values. RF is a machine learning classification and regression model that does not make any assumption about the data to be modelled and can fit non-linear regressions. RF has two parameters that the user needs to set; however, the method is quite insensitive to their values, being the default values optimal in most cases (Liaw and

Wiener 2002), so those default values were used.

The error was the dependent variable, and two predictors were used: 1) Difference between the daily thermal amplitude (dif-AT-Y for AQUA and dif-AT-O for TERRA) and 2) a cosine transformation of julian day (*cdayt*):

$$cdayt = cos\left([t_D - t_C] \cdot \frac{2\pi}{365}\right) \quad (14)$$

Where t_D is the julian day and t_C is the julian day of the coldest day in the year; this predictor is a harmonic function ranging from -1 in the hottest day to 1 in the coolest day. The objective is to check if the error depends on the period of the year.

This correction was only applied to the results obtained for the models TDTM-NDVI-Y and TDTM-NDVI-O, as the results obtained by these models are more accurate than the results of the models TDTM-EVI-Y and TDTM-EVI-O.

2.5. Goodness of fit

The following statistics were used to analyse the fit of the modelled values of ETa:

- Root Mean Square Error (RMSE), which is defined as:

$$RMSE = \sqrt{\frac{1}{n}\sum_{i=1}^{n}(E_i - O_i)^2} \quad (15)$$

- Percentage Bias (PBIAS), which is defined as:

$$PBIAS = \frac{\sum_{i=1}^{n}(E_i - O_i)}{\sum_{i=1}^{n}(O|i)\cdot 100} \quad (16)$$

- Mean Absolute Error (MAE), which is defined as:

$$MAE = \frac{1}{n}\sum_{i=1}^{n}[E_i - O_i] \quad (17)$$

E_i and O_i are respectively the modelled and observed values of ETa.

3. Results

ETa values were obtained using the TDTM model, for all days with available surface temperature (both at the daytime and nighttime pass of the TERRA and AQUA satellites), vegetation indices (NDVI and EVI), albedo and with an average cloudiness fraction during the daytime lower than 20%. These conditions are met in 302 days in the ES-LJu flux tower, but only in 225 days in ES-Amo. The goodness-of-fit analysis of the modelled values of ETa were performed only for those days with modelled values of ETa for both satellites.

Table 3 shows the error statistics of the different variations of the proposed TDTM model. The fit for both satellites is very similar. Likewise, no significant differences are observed between the two values used for ϕ_{max}, with slightly better results being obtained when a value of 1.26 is used. However, when considering the methodology used to obtain vegetation cover fraction, important differences are observed. A much better fit is obtained with Carlson *et al.* (1995) approach than with Minacapilli *et al.* (2016) original methodology. RMSE ranges from 0.65 to 0.97 in the first case and from 1.29 to 2.75 in the second case.

Table 3. Summary of the goodness of fit statistics of the ETa values estimated from the different variations proposed.

	ES-LJu						ES-Amo					
	ϕmax = 1.26			ϕmax = 1.35			ϕmax = 1.26			ϕmax = 1.35		
Model	**MAE**	**RMSE**	**PBIAS**	**MAE**	**RMSE**	**PBIAS**	**MAE**	**RMSE**	**PBIAS**	**MAE**	**RMSE**	**PBIAS**
TDTM-NDVI-Y	0.52	0.68	81	0.58	0.75	93	0.68	0.90	147	0.73	0.97	165
TDTM-NDVI-O	0.50	0.65	79	0.56	0.72	91	0.66	0.89	140	0.71	0.96	157
TDTM-EVI-Y	2.15	2.51	381	2.38	2.75	420	0.98	1.29	229	1.07	1.40	252
TDTM-EVI-O	2.18	2.53	386	2.35	2.75	416	1.00	1.32	233	1.09	1.43	257

The largest errors in the estimation of ETa for both satellites occur in Summer and with daily thermal amplitude values below the mean monthly thermal amplitude. On these days there is an overestimation of the ETa. This tendency also appears, but less importantly, in the rest of the year. The reason of this overestimation is that the TDTM model assumes that areas with lower thermal amplitudes than the mean value for that day of the year would have wetter soils. However, this assumption is not fulfilled in the usually dry summers on the study area.

Figure 4 shows the effects of both variables when modelling the error of the TDTM-NDVI-Y and TDTM-NDVI-O models with RF. Errors increase gradually as *cdayt* approaches - 1, so the highest errors occur in Summer. The more negative are dif-AT-Y or dif-AT-O the higher the error, so they are minimize when these differences are close to zero or positive.

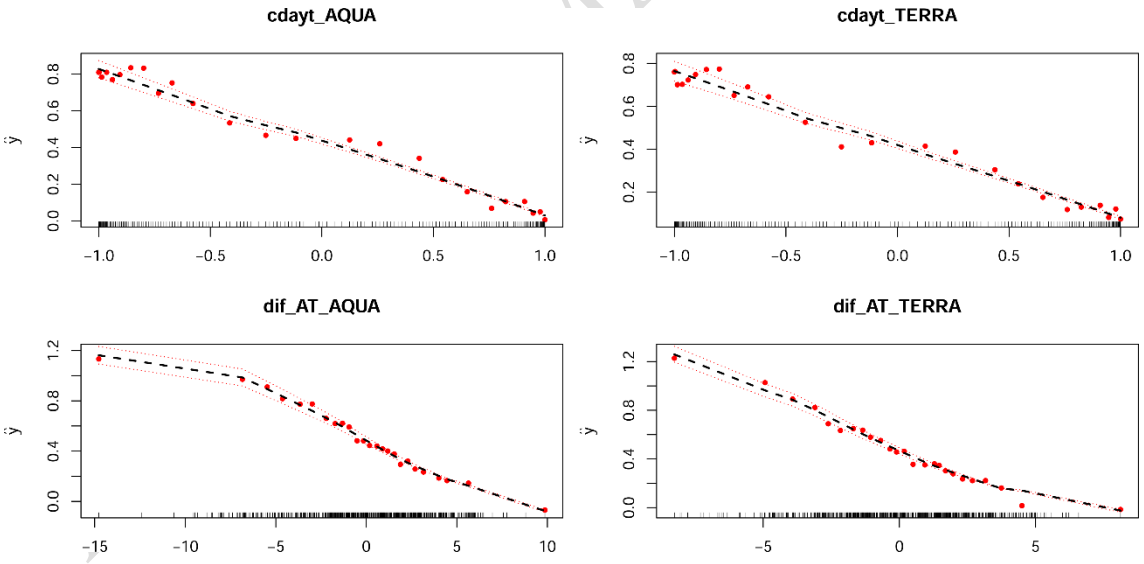

Figure 4. Effects of the predictors used in the RF model to correct the TDTM-NDVI-Y and TDTM-NDVI-O model.

The calibration of the RF model used to correct the error of TDTM-NDVI-Y and TDTM-NDVI-O models was carried out for every day with data in the years 2012 and 2013 (207 from ES-LJu and 131 from ES-Amo). As cloudiness is more common in the

study area in autumn, spring and winter, 42% of the data used in the calibration/validation process belong to the Summer period. The validation was carried out using the available data for 2014 (95 days from ES-LJu and 81 from ES-Amo).

To obtain corrected Eta values, the errors predicted by RF are subtracted from the ETa values estimated with the TDTM-NDVI-Y and TDTM-NDVI-O models.

Corrections improved significantly the performance of both models in the two flux-towers (Table 4). Figure 5 shows a box plot with the observed and modelled values for both satellites, both for the TDTM-NDVI-Y and TDTM-NDVI-O models (O and Y in the Figure 5) and for the correction we proposed (O-corr and Y-corr in the Figure 5).

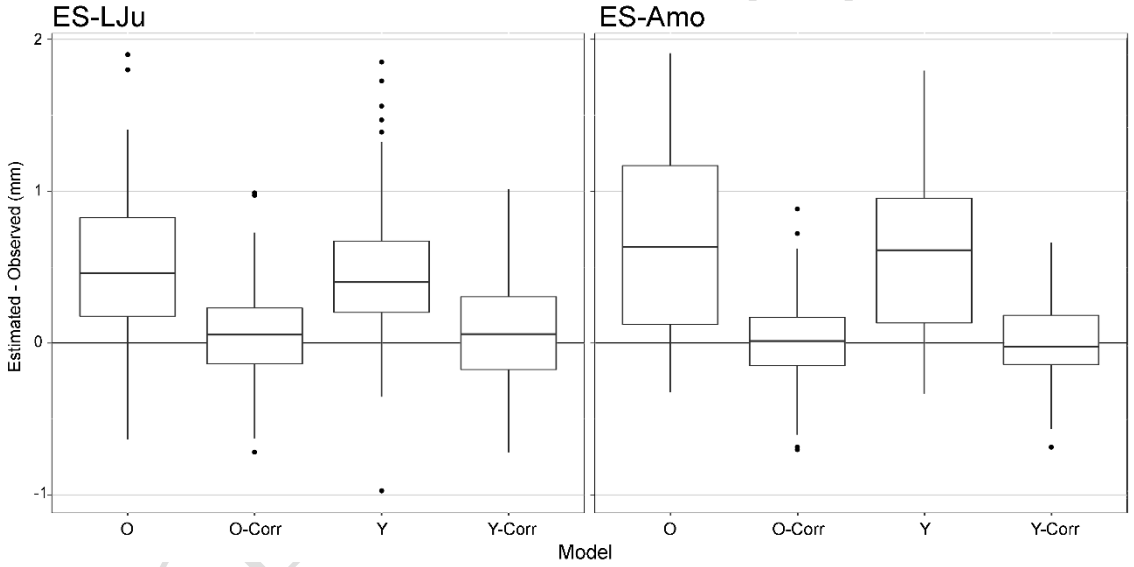

Figure 5. Comparison of the statistics obtained for the TDTM-NDVI-Y and TDTM-NDVI-O models and their respective corrections. Values of the validation series, corresponding to the year 2014.

Table 4. Summary of the goodness of fit statistics of the ETa values estimated from the different variations proposed.

	No corrected			**Corrected**		
Model/Flux tower	**MAE**	**RMSE**	**PBIAS**	**MAE**	**RMSE**	**PBIAS**
TDTM-NDVI-Y/ES-LJu	0.54	0.67	87	0.28	0.35	12
TDTM-NDVI-O/ES-LJu	0.5	0.64	83	0.24	0.31	10
TDTM-NDVI-Y/ES-Amo	0.85	1.02	253	0.24	0.3	47
TDTM-NDVI-O/ES-Amo	0.79	0.97	233	0.27	0.34	46

Figure 6 compares the cumulative ETa values for the year 2014 obtained using TDTM-NDVI-O models and the proposed corrections, and the cumulative ETa values estimated in the flux towers. Figure 6 also shows daily ETa values both observed and estimated. The results obtained for the TDTM-NDVI-Y model are very similar. It is salient the strong reduction in the systematic bias present in the non-corrected estimations.

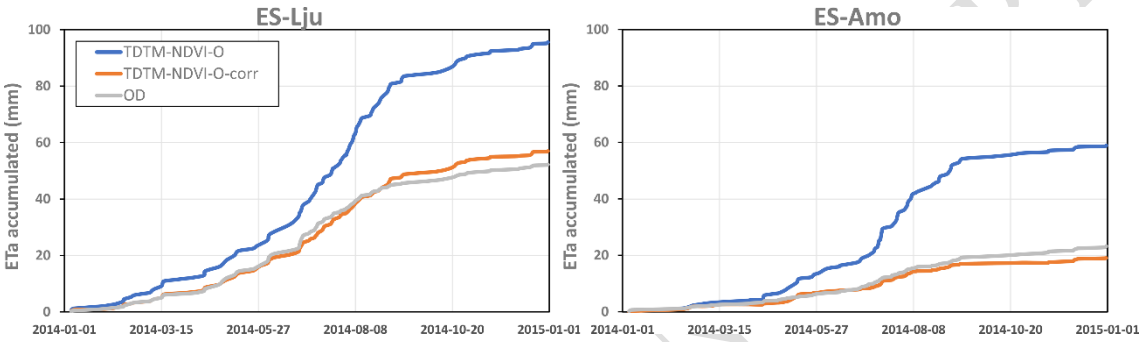

Figure 6. Accumulated ETa (mm) during the year 2014 for the days that meet the criteria established in this work. Observed data (OD), data estimated with TDTM-NDVI-O and with TDTM-NDVI-O-corr are shown.

Table 4, and Figures 5 and 6 show the noteworthy improvement in the fit of the estimated values after applying the proposed correction. Although the difference between the estimated values from both satellites for the whole data set is very small, Table 5 shows that on a daily scale there are differences between the estimated values for both satellites. This table includes different percentiles of the differences between the modelled TDTM-NDVI-Y and TDTM-NDVI-O values and their respective corrections for both flux towers. These differences are reduced after correction. No differences appear among the two satellites, so they could be used indistinctly. The existence of differences between the modelled values on a daily scale would make it advisable to study in the future the use of different criteria for the selection of the ETa values from one satellite or the other on those days for which both are available.

Table 5. Percentiles of the differences between estimated values for both satellites using TDTM-NDVI-Y and TDTM-NDVI-O models and their corrections.

Flux tower	min	P10	P25	P50	P75	P90	max
No corrected							
ES-LJu	0.02	0.03	0.07	0.14	0.26	0.38	1.04
ES-Amo	0.01	0.03	0.09	0.15	0.26	0.4	0.73
Corrected							
ES-LJu	0.01	0.03	0.1	0.32	0.64	0.96	1.47
ES-Amo	0.01	0.03	0.12	0.22	0.55	0.91	1.33

On the other hand, a positive PBIAS was obtained for all the proposed variations and for both flux towers, which indicates an overestimation of ETa, although in TDTM-NDVI-Y-corr and TDTM-NDVI-O-corr models in the ES-LJu flux tower this overestimation is very small (PBIAS = 10 - 12). The highest PBIAS values were obtained for the TDTM-EVI-(Y-O) models with for ϕ_{max} = 1.35 in the ES-LJu flux tower (PBIAS = 416-420).

The spatial distribution of ETa values in Spring and Autumn according to the TDTM-NDVI-(O-Y) method (Figures 7 and 8) is coherent with the characteristics of the study area. The highest values of ETa are recorded in the mountain areas where rainfall is more intense and the NDVI index is higher (higher evaporation and transpiration). In winter, very low values of ETa are obtained using TDTM-NDVI-(O-Y), with few exceptions they do not exceed 0.5 mm, which is consistent with the coldest time of the year. Finally, summer values are the highest and are similar in many areas to those obtained for the same period in the ES-LJu flux tower. In general, the values of ETa obtained from the AQUA satellite data are slightly higher than those obtained from the TERRA satellite.

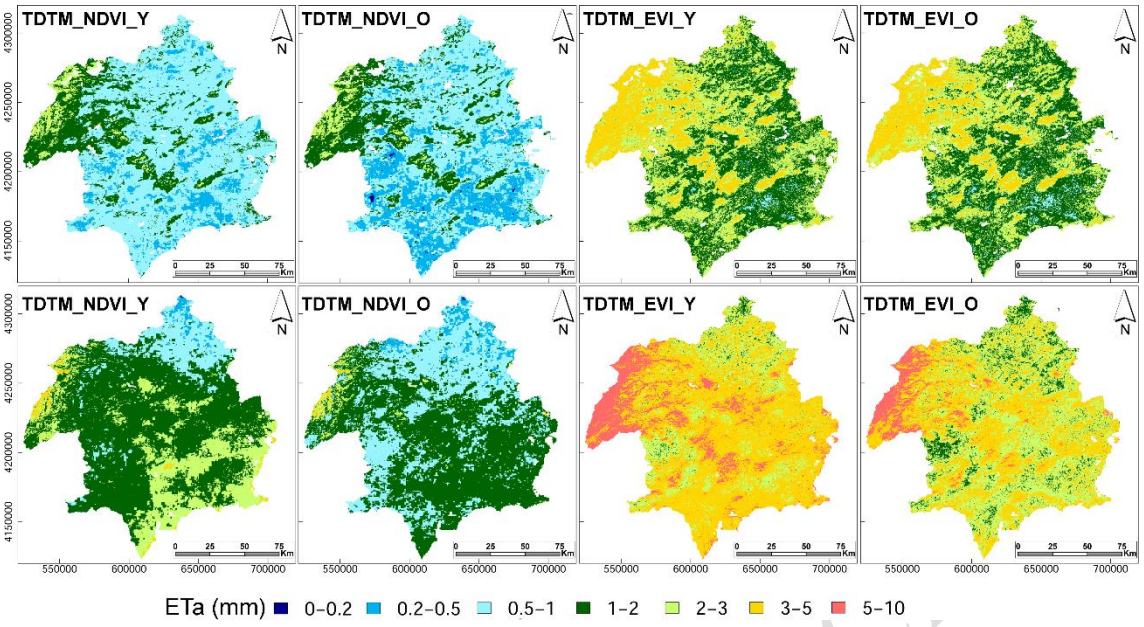

Figure 7. $ET_{a,D}$ maps produced by the TDTM models in Spring (upper row) and Summer (lower row).

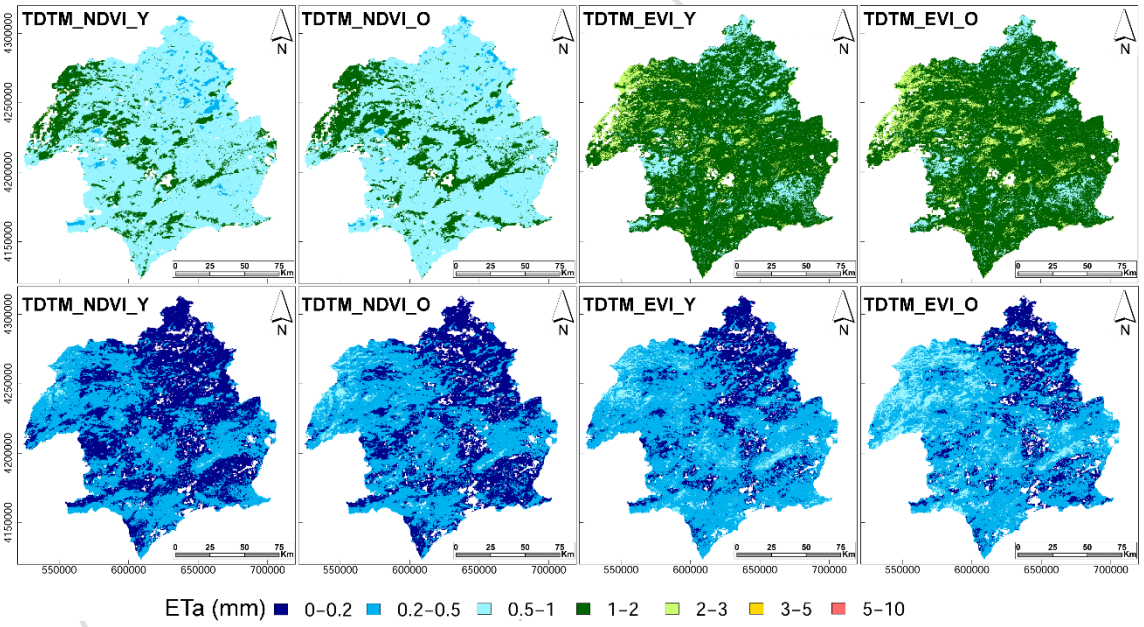

Figure 8. $ET_{a,D}$ maps produced by the TDTM models in Autumn (upper row) and Winter (lower row).

ETa estimations obtained using the TDTM-NDVI-Y or TDTM-NDVI-O models are much better than those obtained with the TDTM-EVI-Y or TDTM-EVI-O models in both flux towers. The reason is that the maximum values of NDVI (0.35 in ES-LJu and 0.42 in ES-Amo), producing F_C values between 0 and 0.05 in ES-LJu and between 0 and

0,11 in ES-Amo. Because of these low values of F_C, ϕ values depend mainly on the daily thermal amplitude and reach the smallest values in Summer, when the daily thermal amplitude is higher. This effect reduces the overestimation of ETa. However, this effect does not appear when using the original methodology of the TDTM method to obtain F_C (Equation (4)).

Figure 9 was obtained with ES-LJu and ES-Amo data for the TERRA satellite with ϕ_{max}=1.26. The orange dots show the ϕ parameter estimated using NDVI, while the blue dots show ϕ estimated with the original, EVI based, methodology. In ES-Amo the values of ϕ are slightly lower than in ES-LJu, while they are similar when obtained with TERRA or AQUA satellites. Figure 9 also shows that the ϕ parameter based on NDVI has a clear temporal pattern, with the highest values in months with low insolation and the lowest values in the months with the highest insolation and, therefore, the greatest daily thermal amplitude. The high values of the ϕ parameter in the coldest months do not cause an overestimation of the ETa because the available energy (*Rn* - *G*) is very low.

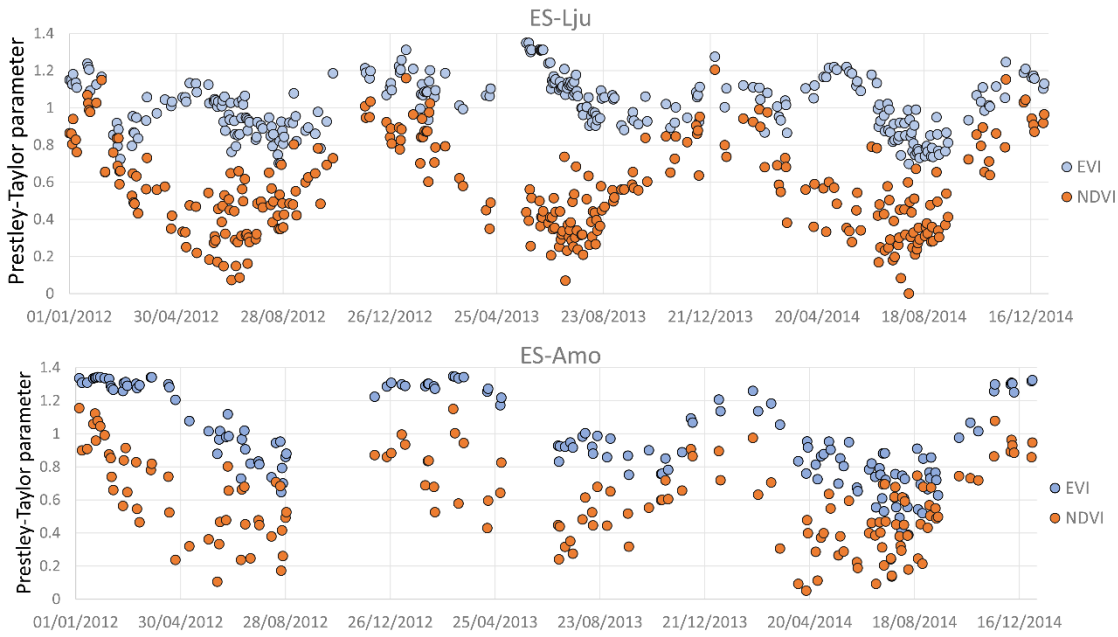

Figure 9. ϕ values in relation with the methodlogy used to calculate F_C.

In the original (TDTM-EVI) methodology, Equation (4) produces FC values that range between 0 (for minimum EVI) and 1 (for maximum EVI). Moreover, with EVI values just 0.03 higher than the minimum EVI the F_C value is above 0.5. This means, as can be seen in Figure 9, that on most days the parameter ϕ is above 0.5, reaching values close to ϕ_{max} in late spring and early summer, when, as occurs in ES-LJu and many points of the DHS, the EVI values are close to the maximum EVI value. When this occurs, the very high ϕ values cause a significant overestimation of ETa (Figure 10). Such Figure represents daily ETa values obtained with ES-LJu data, TDTM-EVI-Y and TDTM-NDVI-Y methods and with ϕ_{max}=1.26. The blue dots represent the values obtained using the TDTM-EVI method and the orange dots present the values obtained using the TDTM-NDVI method, and the green dots (TF) represent the ETa values measured at the ES-LJu flux tower.

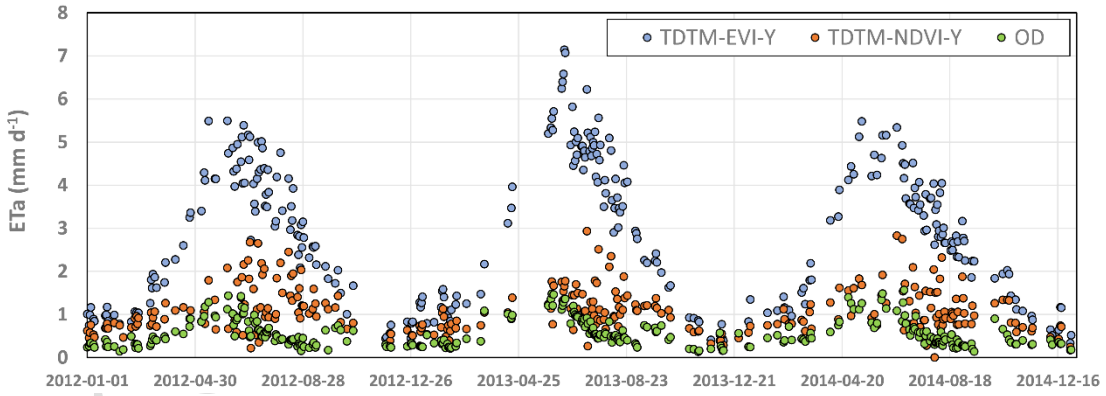

Figure 10. Daily ETa values and TDTM-NDVI-Y and TDTM-EVI-Y estimations in the ES-LJu flux tower.

4. Discussion

Minacapilli *et al.* (2016) obtained, averaging two flux towers, a BIAS of -0.4 mm and an RMSE of 0.70 mm, the latter value being considerably lower than the RMSE of 2.75 mm obtained in the present study for ES-LJu and also lower, although with a smaller difference, than the RMSE of 1.43 mm obtained for ES-Amo. However, our results with

TDTM-NDVI-O and TDTM-NDVI-Y have similar RMSE to theirs (0.73 mm for ES-LJu and 0.96 mm for ES-Amo). The locations of flux towers are not comparable, olive and orange tree crops in Minacapilli *et al.* (2016) whereas ES-LJun is located in a shrubland area and ES-Amo in a grassland area. Furthermore, we obtained ETa values only for clear days, unlike Minacapilli *et al.* (2016) where ETa values were obtained for all days, in the form of 8-day average values.

The ES-LJu flux tower has been used in numerous studies to obtain ETa. A summary of the results obtained in these studies is shown in Table 6. The TDTM-NDVI-O-corr method we used has the lowest RMSE value of all the methods compared. The TDVI quantile 99.99-0.001% method, based on the Temperature-Vegetation Dryness Index (TDVI) and the Priestley-Taylor equation, is the most similar to the TDTM-NDVI model. The PML-measured SWC method is based on the Penman-Monteith-Leuning equation (Leuning *et al.* 2008) and the LAI index. Morillas *et al.* (2013) applied it based on field measurements of net radiation, which can lead to an overestimation of ETa values. Furthermore, this method requires the optimisation of two parameters, which may hamper its use at regional scales. Although the SEBAL method, is one of the methods with lower RMSE, it has the main disadvantage of requiring the calculation of aerodynamic drag. The MOD16 and LSA-SAF-MSG methods are two of the most widely used global models for obtaining ETa. Hu *et al.* (2015) obtained the worst results in Europe for both methods in semi-arid areas such as the DHS, being the only areas where they obtain a correlation coefficient of less than 0.8. The MIKE-SHE SVAT scheme (Brisson *et al.* 2003) is the only hydrological model that appears in the table. It requires a large number of meteorological variables and parameters related to vegetation and soil, which makes its application at regional scales complex (Andersen 2008).

Table 6. RMSE of ETa estimated in the ES-LJu flux tower in other studies.

Method	Temporal scale	RN calculation	RMSE (mm)	Temporal range	Reference
TDTM-NDVI(O-Y)	1 day	Modelled	0.64-0.67	2012-2014	This study
TDTM-NDVI-corr(O-Y)	1 day	Modelled	0.31-0.35	2012-2014	This study
TVDI quantile 99.99-0.001%	8 days	Field data	0.64	2008	Garcia et al. (2014)
PML-measured SWC	1 day	Field data	0.33	2005-2007	Morillas et al. (2013)
SEBAL	1 day	Modelled	0.34	2005-2006	Andersen (2008)
MOD16	8 days	Modelled	0.4	2011	Hu et al. (2015)
LSA-SAF MSG	8 days	Modelled	0.68	2011	Hu et al. (2015)
MIKE SHE SVAT	30 min	Modelled	0.37	2005-2006	Andersen (2008)

For the ES-Amo station, we only found results from the global models MOD16 and LSA-SAF MSG. With RMSE values in 2011 of 0.33 and 0.46 mm, respectively. These values are similar to the RMSE of 0.30 and 0.34 mm obtained in this study for the TDTM-NDVI-Y-corr and TDTM-NDVI-O-corr models.

5. Conclusions

This paper proposes a framework to estimate ETa in a spatially distributed manner in semiarid Mediterranean environments using the TDTM model and two variations of it, and to identify which has the best fit to the validation data. The correction of systematic errors using Random Forest (RF) is also proposed. Validation data come from two flux towers located in scrubland semiarid areas. One of them: ES-LJu has been widely used for the validation of ETa estimation models using remotely sensed data.

According to the validation results, the original TDTM method is significantly worse than in the literature. However, the results obtained with the proposed variation corrected with RF (TDTM-NDVI-corr(-O-Y) models) are very promising for both flux

towers (RMSE between 0.31 and 0.35). Especially considering the simplicity of the model implementation.

A detailed analysis of the validation results shows that the uncorrected models, TDTM-EVI(-O-Y) and TDTM-EVI(-O-Y), have a similar fit independently of the satellite used. Similarly, neither the use of the original Priestley-Taylor value nor the proposed by Minacapilli *et al.* (2016) for semi-arid areas lead to a change in the fit. However, an improvement in the fit is observed when using NDVI as an alternative to estimate F_C (TDTM-NDVI-(O-Y) variations).

However, ETa modelled by the TDTM-NDVI-(O-Y) variations is overestimated in days when the daily thermal amplitude is lower than the monthly mean thermal amplitude, especially in the hottest period of the year. A RF model was proposed to analyse these errors taking into account both factors.

RF correction significantly improved the fit (TDTM-NDVI-corr(-O-Y) variations), reducing the bias and decreasing the dispersion of the errors with respect to the observed values. Regarding the temporal distribution of the errors, it is clear how the largest differences occur in summer in all variations, being corrected to a large extent when using *cdayt* and dif_AT as covariates in RF. Regarding the spatial distribution of the results obtained in the variations, we observe a pattern consistent with the characteristics of the study area, with higher values in mountainous areas, in accordance with the existing rainfall pattern in the DHS, which increases in a SE-NW direction.

However, although the results obtained demonstrate the improvement using the proposed variations, in future work, it would be necessary to evaluate the TDTM-NDVI-(-O-Y) models with a larger number of observed data, ideally with different vegetation and climate conditions, in order to confirm this conclusion and to implement this correction at a regional scale.

Acknowledgments

This work was supported by the Spanish Ministry of Economy, Industry and Competitiveness/Agencia Estatal de Investigación/FEDER [grant number CGL2017-84625-C2-2-R].

We thank Prof. Enique Perez Sanchez-Cañete (University of Granada) to provide the flux towers data, supported by Junta de Andalucía-Consejería de Economía y Conocimiento/FEDER [Proyect PESA2, grant number A-RNM-318-UGR18]. We also thank the Associate Editor and anonymous reviewers for their constructive comments and suggestions that improved this paper greatly.

Declaration of interest statement

The authors declare that they have no known competing financial interests or personal relationships that could have appeared to influence the work reported in this paper.

Disclosure statement

No potential conflict of interest was reported by the author(s).

Data availability statement

The data that support the findings of this study are available from the corresponding author, [F. G.-C.], upon reasonable request.

References

Allen, R.G., Pereira, L.S., Howell, T.A. & Jensen, M.E., 2011. Evapotranspiration information reporting: I. Factors governing measurement accuracy. *Agricultural Water Management*, 98 (6), 899-920.

Allen, R.G., Pereira, L.S., Raes, D. & Smith, M., 2006. *Evapotranspiración del cultivo: Guias para la determinación de los requerimientos de agua de los cultivos*: FAO.

Allen, R.G., Tasumi, M., Morse, A., Trezza, R., Wright, J.L., Bastiaanssen, W., Kramber, W., Lorite, I. & Robison, C.W., 2007a. Satellite-based energy balance for mapping evapotranspiration with internalized calibration (metric)—applications. *Journal of Irrigation and Drainage Engineering,* 133 (4), 395-406.

Allen, R.G., Tasumi, M. & Trezza, R., 2007b. Satellite-based energy balance for mapping evapotranspiration with internalized calibration (metric)—model. *Journal of Irrigation and Drainage Engineering,* 133 (4), 380-394.

Andersen, F.H., 2008. *Hydrological modeling in a semi-arid area using remote sensing data*. University of Copenhagen.

Anderson, M.C., Norman, J.M., Mecikalski, J.R., Otkin, J.A. & Kustas, W.P., 2007. A climatological study of evapotranspiration and moisture stress across the continental United States based on thermal remote sensing: 2. Surface moisture climatology. *Journal of Geophysical Research,* 112 (D11), D11112.

Beigi, E. & Tsai, F.T.C., 2014. Gis-based water budget framework for high-resolution groundwater recharge estimation of large-scale humid regions. *Journal of Hydrologic Engineering,* 19 (8), 05014004.

Breiman, L., 2001. Random Forests. *Machine learning,* 45 (1), 5--32.

Brisson, N., Gary, C., Justes, E., Roche, R., Mary, B., Ripoche, D., Zimmer, D., Sierra, J., Bertuzzi, P., Burger, P., Bussire, F., Cabidoche, Y.M., Cellier, P., Debaeke, P., Gaudillre, J.P., Hnault, C., Maraux, F., Seguin, B. & Sinoquet, H., 2003. An overview of the crop model stics. *European Journal of Agronomy,* 18 (3-4), 309--332.

Carlson, T.N., Capehart, W.J. & Gillies, R.R., 1995. A new look at the simplified method for remote sensing of daily evapotranspiration. *Remote Sensing of Environment,* 54 (2), 161--167.

CHS, 2015. *Plan hidrológico de la Demarcación Hidrográfica del Segura. Ciclo de planificación hidrológica 2015-2021*.

Cleugh, H.A., Leuning, R., Mu, Q. & Running, S.W., 2007. Regional evaporation estimates from flux tower and MODIS satellite data. *Remote Sensing of Environment,* 106 (3), 285-304.

Conesa-García, C. & Alonso-Sarría, F., 2006. El clima de la Región de Murcia. *El medio físico de la Región de Murcia.* Editum, 95-128.

Didan, K., 2015. Mod13q1 MODIS/TERRA vegetation indices 16-day l3 global 250m sin grid v006. *NASA EOSDIS Land Processes DAAC*.

Fisher, J.B., Tu, K.P. & Baldocchi, D.D., 2008. Global estimates of the land--atmosphere water flux based on monthly avhrr and islscp-ii data, validated at 16 fluxnet sites. *Remote Sensing of Environment,* 112 (3), 901-919.

García, M., Fernández, N., Villagarca, L., Domingo, F., Puigdefábregas, J. & Sandholt, I., 2014. Accuracy of the temperature--vegetation dryness index using MODIS under

water-limited vs. Energy-limited evapotranspiration conditions. *Remote Sensing of Environment,* 149, 100-117.

Gavahi, K., Abbaszadeh, P., Moradkhani, H., Zhan, X. & Hain, C., 2020. Multivariate assimilation of remotely sensed soil moisture and evapotranspiration for drought monitoring. *Journal of Hydrometeorology,* 21 (10), 2293-2308.

Glenn, E.P., Huete, A.R., Nagler, P.L., Hirschboeck, K.K. & Brown, P., 2007. Integrating remote sensing and ground methods to estimate evapotranspiration. *Critical Reviews in Plant Sciences,* 26 (3), 139-168.

Gomariz-Castillo, F., 2016. *Estimación de variables y parámetros hidrológicos y análisis de su influencia sobre la modelización hidrológica: Aplicación a los modelos de Témez y Swat*. University of Murcia.

Herman, M.R., Nejadhashemi, A.P., Abouali, M., Hernandez-Suarez, J.S., Daneshvar, F., Zhang, Z., Anderson, M.C., Sadeghi, A.M., Hain, C.R. & Sharifi, A., 2018. Evaluating the role of evapotranspiration remote sensing data in improving hydrological modeling predictability. *Journal of Hydrology,* 556, 39-49.

Hu, G., Jia, L. & Menenti, M., 2015. Comparison of MOD16 and LSA-SAF MSG evapotranspiration products over Europe for 2011. *Remote Sensing of Environment,* 156, 510--526.

Jamshidi, S., Zand-Parsa, S., Naghdyzadegan Jahromi, M. & Niyogi, D., 2019a. Application of a simple Landsat-MODIS fusion model to estimate evapotranspiration over a heterogeneous sparse vegetation region. *Remote Sensing,* 11 (7).

Jamshidi, S., Zand-Parsa, S., Pakparvar, M. & Niyogi, D., 2019b. Evaluation of evapotranspiration over a semiarid region using multiresolution data sources. *Journal of Hydrometeorology,* 20 (5), 947-964.

Jiang, L. & Islam, S., 2001. Estimation of surface evaporation map over southern great plains using remote sensing data. *Water resources research,* 37 (2), 329-340.

Kalma, J.D., Mcvicar, T.R. & Mccabe, M.F., 2008. Estimating land surface evaporation: A review of methods using remotely sensed surface temperature data. *Surveys in Geophysics,* 29 (4-5), 421-469.

Kustas, W.P. & Daughtry, C.S.T., 1990. Estimation of the soil heat flux/net radiation ratio from spectral data. *Agricultural and Forest Meteorology,* 49 (3), 205--223.

Leuning, R., Zhang, Y.Q., Rajaud, A., Cleugh, H. & Tu, K., 2008. A simple surface conductance model to estimate regional evaporation using MODIS leaf area index and the Penman-Monteith equation. *Water Resources Research,* 44 (10).

Li, Z.-L., Tang, R., Wan, Z., Bi, Y., Zhou, C., Tang, B., Yan, G. & Zhang, X., 2009. A review of current methodologies for regional evapotranspiration estimation from remotely sensed data. *Sensors,* 9 (5), 3801-3853.

Liaw, A. & Wiener, M., 2002. Classification and regression by RandomForest. *R News*, 2 (3), 18--22 Available from: https://cran.r-project.org/doc/Rnews/.

López-Ballesteros, A., Serrano-Ortiz, P., Kowalski, A.S., Sánchez-Cañete, E.P., Scott, R.L. & Domingo, F., 2017. Subterranean ventilation of allochthonous CO^2 governs net co2 exchange in a semiarid Mediterranean grassland. *Agricultural and Forest Meteorology*, 234-235, 115-126.

Lorenz, D.J., Otkin, J.A., Svoboda, M., Hain, C.R., Anderson, M.C. & Zhong, Y., 2017. Predicting u.S. Drought monitor states using precipitation, soil moisture, and evapotranspiration anomalies. Part i: Development of a nondiscrete usdm index. *Journal of Hydrometeorology*, 18 (7), 1943-1962.

Minacapilli, M., Consoli, S., Vanella, D., Ciraolo, G. & Motisi, A., 2016. A time domain triangle method approach to estimate actual evapotranspiration: Application in a Mediterranean region using MODIS and MSG-SEVIRI products. *Remote Sensing of Environment*, 174, 10-23.

Minhas, P.S., Ramos, T.B., Ben-Gal, A. & Pereira, L.S., 2020. Coping with salinity in irrigated agriculture: Crop evapotranspiration and water management issues. *Agricultural Water Management*, 227, 105832.

Miralles, D.G. & Holmes, T.R.H.A., 2011. Global land-surface evaporation estimated from satellite-based observations. *Hydrology and Earth System Sciences*, 15 (2), 453.

Monteith, J. & Unsworth, M., 2013. *Principles of environmental physics*, Fourth Edition ed. Boston: Academic Press.

Morillas, L., Leuning, R., Villagarca, L., Garca, M., Serrano-Ortiz, P. & Domingo, F., 2013. Improving evapotranspiration estimates in Mediterranean drylands: The role of soil evaporation. *Water Resources Research*, 49 (10), 6572--6586.

Mu, Q., Zhao, M. & Running, S.W., 2011. Improvements to a MODIS global terrestrial evapotranspiration algorithm. *Remote Sensing of Environment*, 115 (8), 1781-1800.

Myneni, R., Knyazikhin, Y. & Park, T., 2015. Mcd15a2h MODIS/TERRA+AQUA leaf area index/fpar 8-day l4 global 500m sin grid v006. *NASA EOSDIS Land Processes DAAC*.

Niyogi, D., Jamshidi, S., Smith, D. & Kellner, O., 2020. Evapotranspiration climatology of Indiana using in situ and remotely sensed products. *Journal of Applied Meteorology and Climatology*, 59 (12), 2093-2111.

Norman, J.M., Anderson, M.C., Kustas, W.P., French, A.N., Mecikalski, J., Torn, R., Diak, G.R., Schmugge, T.J. & Tanner, B.C.W., 2003. Remote sensing of surface energy fluxes at 10^1-m pixel resolutions. *Water Resources Research*, 39 (8), 1221.

Norman, J.M., Kustas, W.P. & Humes, K.S., 1995. Source approach for estimating soil and vegetation energy fluxes in observations of directional radiometric surface temperature. *Agricultural and Forest Meteorology*, 77 (3), 263-293.

Pastorello, G., Trotta, C., Canfora, E. & Al., E., 2020. The fluxnet2015 dataset and the oneflux processing pipeline for eddy covariance data. *Nature Scientific Data,* 7, 225.

Pereira, L.S., Allen, R.G., Smith, M. & Raes, D., 2015. Crop evapotranspiration estimation with \ fao \ 56: Past and future. *Agricultural Water Management,* 147, 4-20.

Pourmansouri, F. & Rahimzadegan, M., 2020. Evaluation of vegetation and evapotranspiration changes in Iran using satellite data and ground measurements. *Journal of Applied Remote Sensing,* 14 (3), 1-1.

Price, J.C., 1990. Using spatial context in satellite data to infer regional scale evapotranspiration. *IEEE transactions on Geoscience and Remote Sensing,* 28 (5), 940-948.

Priestley, C.H.B. & Taylor, R.J., 1972. On the assessment of surface heat flux and evaporation using large-scale parameters. *Monthly weather review,* 100 (2), 81-92.

Prihodko, L. & Goward, S.N., 1997. Estimation of air temperature from remotely sensed surface observations. *Remote Sensing of Environment,* 60 (3), 335-346.

Rahimpour, M. & Rahimzadegan, M., 2021. Assessment of surface energy balance algorithm for land and operational simplified surface energy balance algorithm over freshwater and saline water bodies in Urmia lake basin. *Theoretical and Applied Climatology,* 143 (3), 1457-1472.

Roerink, G.J., Su, Z. & Menenti, M., 2000. S-sebi: A simple remote sensing algorithm to estimate the surface energy balance. *Physics and Chemistry of the Earth, Part B: Hydrology, Oceans and Atmosphere,* 25 (2), 147-157.

Ruiz-Álvarez, M., Alonso-Sarría, F. & Gomariz-Castillo, F., 2020. Interpolation of instantaneous air temperature using geographical and MODIS derived variables with machine learning techniques. *ISPRS International Journal of Geo-Information,* 8 (9), 382.

Schaaf, C. & Wang, Z., 2015. Mcd43a4 MODIS/TERRA+AQUA brdf/albedo nadir brdf adjusted ref daily l3 global - 500m v006. *NASA EOSDIS Land Processes DAAC*.

Senay, G.B., Bohms, S., Singh, R.K., Gowda, P.H., Velpuri, N.M., Alemu, H. & Verdin, J.P., 2013. Operational evapotranspiration mapping using remote sensing and weather datasets: A new parameterization for the sseb approach. *JAWRA Journal of the American Water Resources Association,* 49 (3), 577-591.

Serrano-Ortiz, P., Domingo, F., Cazorla, A., Were, A., Cuezva, S., Villagarcía, L. & Alados-Arboledas, L.K., A.S., 2009. Interannual co2 exchange of a sparse mediterranean shrubland on a carbonaceous substrate. *Journal of Geophysical Research,* 114, G04015.

Serrano-Ortiz, P., Kowalski, A.S., Domingo, F., Rey, A., Pegoraro, E., Villagarcía, L. & Alados-Arboledas, L., 2007. Variations in daytime net carbon and water exchange in a montane shrubland ecosystem in southeast Spain. *Photosynthetica,* 40, 30-35.

Su, Z., 2002. The surface energy balance system (sebs) for estimation of turbulent heat fluxes. *Hydrology and earth system sciences,* 6 (1), 85-100.

Tang, R., Li, Z.-L. & Tang, B., 2010. An application of the t s--vi triangle method with enhanced edges determination for evapotranspiration estimation from MODIS data in arid and semi-arid regions: Implementation and validation. *Remote Sensing of Environment,* 114 (3), 540--551.

Teixeira, A.H.D.C., Bastiaanssen, W.G.M., Ahmad, M.-U.-D. & Bos, M.G., 2009a. Reviewing sebal input parameters for assessing evapotranspiration and water productivity for the low-middle Sao Francisco river basin, brazil: Part a: Calibration and validation. *agricultural and forest meteorology,* 149 (3), 462-476.

Teixeira, A.H.D.C., Bastiaanssen, W.G.M., Ahmad, M.U.-D. & Bos, M.G., 2009b. Reviewing sebal input parameters for assessing evapotranspiration and water productivity for the low-middle Sao Francisco river basin, brazil part b: Application to the regional scale. *Agricultural and Forest Meteorology,* 149, 477-490.

Tian, F., Qiu, G., Yang, Y., Lü, Y. & Xiong, Y., 2013. Estimation of evapotranspiration and its partition based on an extended three-temperature model and MODIS products. *Journal of Hydrology,* 498, 210-220.

Wan, Z., Hook, S. & Hulley, G., 2015a. Mod11a1 MODIS/TERRA land surface temperature/emissivity daily l3 global 1km sin grid v006. *NASA EOSDIS Land Processes DAAC.*

Wan, Z., Hook, S. & Hulley, G., 2015b. Mod11a2 MODIS/AQUA land surface temperature/emissivity 8-day l3 global 1km sin grid v006. *NASA EOSDIS Land Processes DAAC.*

Wan, Z., Hook, S. & Hulley, G., 2015c. Myd11a1 MODIS/AQUA land surface temperature/emissivity daily l3 global 1km sin grid v006. *NASA EOSDIS Land Processes DAAC.*

Wan, Z., Hook, S. & Hulley, G., 2015d. Myd11a2 MODIS/TERRA land surface temperature/emissivity 8-day l3 global 1km sin grid v006. *NASA EOSDIS Land Processes DAAC.*

Wang, Y., Li, R., Hu, J., Wang, X., Kabeja, C., Min, Q. & Wang, Y., 2021. Evaluations of MODIS and microwave-based satellite evapotranspiration products under varied cloud conditions over east asia forests. *Remote Sensing of Environment,* 264, 112606.

Xiao, Z., Liang, S., Wang, J., Xie, D., Song, J. & Fensholt, R., 2015. A framework for consistent estimation of leaf area index, fraction of absorbed photosynthetically active radiation, and surface albedo from MODIS time-series data. *IEEE Transactions on Geoscience and Remote Sensing,* 53 (6), 3178-3197.

Xiong, Y.J. & Qiu, G.Y., 2014. Simplifying the revised three-temperature model for remotely estimating regional evapotranspiration and its application to a semi-arid steppe. *International journal of remote sensing,* 35 (6), 2003-2027.

Xiong, Y.J., Zhao, S.H., Tian, F. & Qiu, G.Y., 2015. An evapotranspiration product for arid regions based on the three-temperature model and thermal remote sensing. *Journal of Hydrology*, 530, 392-404.

Yang, Y., Shang, S. & Jiang, L., 2012. Remote sensing temporal and spatial patterns of evapotranspiration and the responses to water management in a large irrigation district of north china. *Agricultural and forest meteorology*, 164, 112-122.

Yaseen, Z.M., Al-Juboori, A.M., Beyaztas, U., Al-Ansari, N., Chau, K.-W., Qi, C., Ali, M., Salih, S.Q. & Shahid, S., 2020. Prediction of evaporation in arid and semi-arid regions: A comparative study using different machine learning models. *Engineering Applications of Computational Fluid Mechanics*, 14 (1), 70-89.

Zhang, K., Kimball, J.S. & Running, S.W., 2016. A review of remote sensing based actual evapotranspiration estimation. *WIREs Water*, 3 (6), 834-853.

Zhou, X., Bi, S., Yang, Y., Tian, F. & Ren, D., 2014. Comparison of et estimations by the three-temperature model, sebal model and eddy covariance observations. *Journal of Hydrology*, 519, 769-776.

Zhu, W., Jia, S. & Lv, A., 2017. A universal ts-vi triangle method for the continuous retrieval of evaporative fraction from MODIS products. *Journal of Geophysical Research: Atmospheres*, 122 (19), 206-227.